Proc. Natl. Acad. Sci. USA
Vol. 95, pp. 7850–7853, July 1998
Applied Mathematics

The instability of stratified flows at large Richardson numbers

ANDREW J. MAJDA* AND MICHAEL SHEFTER

Courant Institute of Mathematical Sciences, New York University, New York, NY 10012

Contributed by Andrew J. Majda, May 4, 1998

ABSTRACT **In contrast to conventional expectations based on the stability of steady shear flows, elementary time-periodic stratified flows that are unstable at arbitrarily large Richardson numbers are presented here. The fundamental instability is a parametric one with twice the period of the basic state. This instability spontaneously generates local shears on buoyancy time scales near a specific angle of inclination that saturates into a localized regime of strong mixing with density overturning. We speculate that such instabilities may contribute significantly to the step-like microstructure often observed in buoyancy measurements in the ocean.**

One of the basic analytical results for stably stratified fluid flows is the celebrated Miles–Howard theorem (1, 2). This theorem states that steady shear flows $\mathbf{V} = (v(z), 0, 0)$ in an inviscid stably stratified fluid are linearly stable for all Richardson numbers, $\mathcal{R}i$, satisfying

$$\mathcal{R}i > \frac{1}{4}, \quad \mathcal{R}i = \frac{N^2}{\left(\frac{\partial v}{\partial z}\right)^2} \qquad [1]$$

with $N^2 = -g\frac{\partial \rho}{\partial z}/\rho_b$, the square of the buoyancy or Brunt–Vaisala frequency. This criterion for stability is often interpreted and applied literally for time-dependent flow fields in both theoretical and numerical modeling for the atmosphere or ocean. For example, a popular turbulent eddy diffusivity used in numerical simulations in the atmosphere/ocean community is the Lilly–Smagorinsky eddy diffusivity (3, 4), where the turbulent eddy diffusivity is completely switched off and set to zero for $\mathcal{R}i \geq \overline{\mathcal{R}i} \geq \frac{1}{4}$ with $\overline{\mathcal{R}i}$ of order unity. Here, we present elementary examples, with firm mathematical underpinnings, which demonstrate that such reasoning can be violated in dramatic fashion for time-dependent strongly stratified flows. With appropriate nondimensional units explained below, we consider solutions of the inviscid two-dimensional Boussinessq equations in vorticity-stream form,

$$\begin{aligned} \Omega_t + \nabla^\perp\psi \cdot \nabla\Omega &= \tilde{\rho}_x \\ \tilde{\rho}_t + \nabla^\perp\psi \cdot \nabla\tilde{\rho} &= 0 \\ \Delta\psi &= \Omega, \end{aligned} \qquad [2]$$

where $\tilde{\rho}$ is fluid density, $\Omega(x, z, t) = \frac{\partial u}{\partial z} - \frac{\partial w}{\partial x}$ is the vorticity, ψ is the stream function, and the field velocity $\mathbf{v}$ is given by

$$\mathbf{v} = \nabla^\perp\psi = \begin{pmatrix} \partial_z\psi \\ -\partial_x\psi \end{pmatrix}. \qquad [3]$$

Next, we build elementary time-periodic mean states for the equations in **2**, and then we demonstrate their linearized and nonlinear instability for large Richardson numbers.

Time-Periodic Mean States and the Nonlinear Pendulum

We construct elementary time-periodic exact solutions of the Boussinessq equations with constant spatial gradients with the form

$$\begin{aligned} \tilde{\rho} &= \rho_b + \sin\theta(t)x - \cos\theta(t)z \\ \Omega &= \omega(t) \\ \mathbf{V} &= \left(\frac{\omega(t)}{2}z, -\frac{\omega(t)}{2}x\right). \end{aligned} \qquad [4]$$

Direct calculation yields the fact that special solutions of **2** have the structure in **4** provided that the phase function, $\theta(t)$, satisfies the nonlinear pendulum equation

$$2\frac{d^2\theta}{dt^2} = -\sin\theta(t), \quad \omega(t) = -2\frac{d\theta}{dt} \qquad [5]$$

with the initial data

$$\theta(t)\big|_{t=0} = 0, \quad \omega(t)\big|_{t=0} = (\mathcal{R}i)^{-1/2}. \qquad [6]$$

Implicit in both **2** and **6** is a nondimensionalization where we use the ambient density, ρ_b, the stably stratified initial vertical density gradient, and gravity, g, to set the relevant scales. Thus, the unit of time in **2** is determined by the constant buoyancy frequency, N, with the unit of space set by the density gradient. The natural Richardson number from **1** for these mean flows is given by the square of the ratio of the eddy turnover time to the buoyancy time and this results in the nondimensional factor, $(\mathcal{R}i)^{-1/2}$, appearing in the initial data in **6**. We remark that with this definition of the Richardson number, the Froude number, $\mathcal{F}r$, and the Richardson number are related by $\mathcal{F}r = (\mathcal{R}i)^{-1/2}$; this expresses the fact that for $\mathcal{R}i \gg 1$, the stratification is much stronger than the fluid motion and emphasizes the point that the buoyancy time scale, the unit of time use here, is much shorter than the mean eddy turnover time in these elementary flows with strong stratification for $\mathcal{R}i \gg 1$.

The pendulum equation in **5** has the conserved energy, $\mathcal{H} = \dot{\theta}^2 - \cos\theta$, and from **4**, overturning of density occurs provided $\cos\theta(t) < 0$. With this information, it is a simple exercise to check that no overturning occurs in these mean flows precisely for $\mathcal{R}i > \frac{1}{4}$, in rough correspondence with the Miles–Howard theorem; furthermore, the minimum time-dependent Richardson number in these time-periodic flows occurs at the initial time, $t = 0$. These elementary flows admit the following physical interpretation: the initial vortex deflects the initially horizontal isopycnal surfaces to a maximum angle and converts all of its kinetic energy into potential energy in the process; baroclinic vorticity production then converts this potential energy back into kinetic energy and restarts the next phase of the oscillation cycle. For increasing Richardson numbers, the initial vortex is increasingly weak and the deflection angle for the isopycnal surfaces is increasingly small.

If $\xi = (\xi_1, \xi_3)$ marks the initial location, these Lagrangian marker particles evolve by the velocity to new locations $\mathcal{X} = (X(\xi, t), Z(\xi, t))$. For the mean flows satisfying **4**, **5**, and **6**, these particle trajectories are given explicitly by

$$\mathcal{X} = U(t)\xi = \begin{pmatrix} \cos\theta(t) & -\sin\theta(t) \\ \sin\theta(t) & \cos\theta(t) \end{pmatrix}\xi. \qquad [7]$$

The publication costs of this article were defrayed in part by page charge payment. This article must therefore be hereby marked "*advertisement*" in accordance with 18 U.S.C. §1734 solely to indicate this fact.

© 1998 by The National Academy of Sciences 0027-8424/98/957850-4$2.00/0
PNAS is available online at http://www.pnas.org.

*To whom reprint requests should be addressed. e-mail: jonjon@cims.nyu.edu.

To study the stability of these basic time-periodic mean flows, we consider perturbed initial data for the Boussinessq equations in **2** with the form

$$\Omega\big|_{t=0} = (\mathcal{R}i)^{-1/2} + \omega_0'(x,z), \quad \tilde{\rho}\big|_{t=0} = -z + \rho_0'(x,z)$$
$$\omega_0' = (\mathcal{R}i)^{-1/2}\omega_0, \quad \rho_0' = (\mathcal{R}i)^{-1/2}\rho_0. \qquad [8]$$

From **2**, the equations of motion for the evolving perturbations $\omega'(x,z,t)$, $\rho'(x,z,t)$ are given by

$$\omega_t' + \mathbf{V}\cdot\nabla\omega' + \nabla^\perp\psi'\cdot\nabla\omega' = \rho_x'$$
$$\rho_t' + \mathbf{V}\cdot\nabla\rho' + \nabla^\perp\psi'\cdot\nabla\rho' + \nabla^\perp\psi'\cdot\nabla\tilde{\rho} = 0 \qquad [9]$$
$$\Delta\psi' = \omega'.$$

In **9**, $\tilde{\rho}$ arises from the mean flow in **4**. Next, we write the equations in **9** in mean Lagrangian coordinates with **7** to facilitate the stability analysis.

Mean Lagrangian Coordinates

With the explicit transformation in **7**, the equations for the perturbations ρ', ω', in mean Lagrangian coordinates, $\xi = (\xi_1, \xi_3)$, assume the elegant form (dropping the primes)

$$\omega_t + \left(\nabla_\xi^\perp\psi\cdot\nabla_\xi\omega\right) = \left(\cos\theta(t)\partial_{\xi_1} - \sin\theta(t)\partial_{\xi_3}\right)\rho$$
$$\rho_t + \left(\nabla_\xi^\perp\psi\cdot\nabla_\xi\rho\right) + \frac{\partial\psi}{\partial\xi_1} = 0 \qquad [10]$$
$$\Delta_\xi\psi = \omega.$$

Linear Instability and Hill's Equation

We build elementary exact plane wave solutions for the transformed Boussinessq equations in **10** with the form

$$\omega(\xi,t) = \hat{\omega}_k(t)\sin(\mathbf{k}\cdot\xi),$$
$$\rho(\xi,t) = \hat{\rho}_k(t)\cos(\mathbf{k}\cdot\xi). \qquad [11]$$

With the ansatz in **11**, the nonlinear terms $\nabla_\xi^\perp\psi\cdot\nabla_\xi\omega$ and $\nabla_\xi^\perp\psi\cdot\nabla_\xi\rho$ both vanish, and the equations in **10** reduce to the ordinary differential equations for the amplitudes, $\hat{\omega}_k$, $\hat{\rho}_k$, given by

$$\frac{d\hat{\omega}_k}{dt} = -\left[\cos\theta(t)k_1 - \sin\theta(t)k_3\right]\hat{\rho}_k$$
$$\frac{d\hat{\rho}_k}{dt} = \frac{k_1}{|\mathbf{k}|^2}\hat{\omega}_k, \qquad [12]$$

where $\theta(t)$ solves the pendulum equation in **5** and **6**. We note that the equations in **12** are equivalent to the classic Hill's equation (5),

$$\frac{d^2}{dt^2}\hat{\rho}_k = -P(t)\hat{\rho}_k(t),$$
$$P(t) = \frac{k_1}{|\mathbf{k}|^2}\left[k_1\cos\theta(t) - k_3\sin\theta(t)\right]. \qquad [13]$$

To investigate whether perturbations grow in time and have instability, we use elementary Floquet theory for the time-periodic equations in **13**; this theory yields the criterion that for instability, we need to check only that the trace of the Floquet matrix exceeds 2 in magnitude (6). Clearly, the periodic function $P(t)$ in **13** depends on the direction of $\mathbf{k}$ but not on the magnitude of $\mathbf{k}$. Thus, we set $\mathbf{k} = (k_1, k_3) = (\sin\theta_0, -\cos\theta_0)|\mathbf{k}|$, where the angle θ_0 parameterizes this variation in **13**. In Fig. 1, we give an explicit demonstration of instability at arbitrarily large Richardson numbers. In

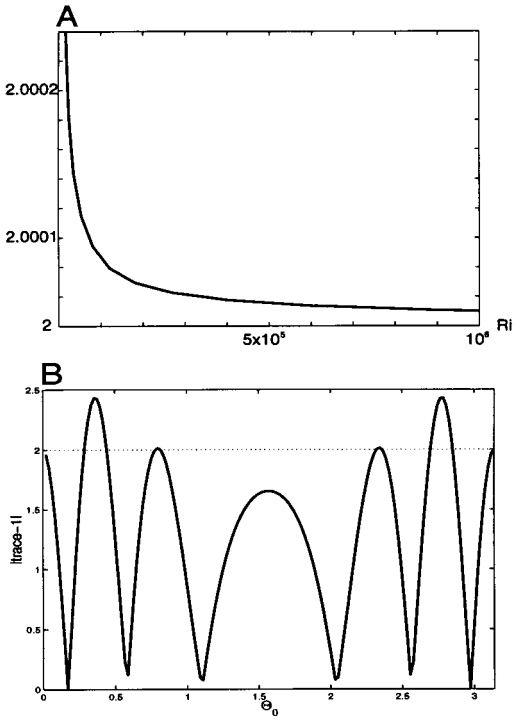

FIG. 1. Maximum trace of Floquet matrix at large values of Richardson number (A) and the trace of Floquet matrix for different inclination angles for fixed Richardson number, $\mathcal{R}i = 5$ (B).

Fig. 1*A*, through numerical evaluation, we graph the value of the Floquet trace, maximized over all angles, θ_0, for Richardson numbers, $1 \leqslant \mathcal{R}i \leqslant 10^6$. Even though the growth rates become extremely small at these large Richardson numbers, nevertheless, there is unambiguous evidence for instability. In Fig. 1*B*, we plot the Floquet trace as a function of the angle θ_0 for the representative moderately large Richardson number $\mathcal{R}i = 5$. Although we do not display this here, the angles θ_0^* with the two peaks in the growth rate correspond to a parametric instability where the instability grows with twice the period of the underlying fluid flow. The qualitative features displayed here for $\mathcal{R}i = 5$ in Fig. 1*B* in fact persist for all Richardson numbers investigated for $\mathcal{R}i > \frac{1}{4}$. Thus, linear instability theory predicts the spontaneous formation of density stratified shears aligned in preferred directions of variation near the direction θ_0^*. How do these instabilities alter the nonlinear dynamics in the stably stratified flow? We address this issue next.

Nonlinear Instability and Density Overturning

To understand the nature of the nonlinear instability, we integrated the mean Lagrangian equations in **10** numerically with a standard pseudo-spectral method (7) on a rectangular $2\pi-$periodic box for $\mathcal{R}i = 5$ with a resolution of $(64)^2$ Fourier modes. We chose random large-scale initial data by assigning equal amplitude and random phases confined to all wave numbers with $|k_i| \leqslant 10$; we set this amplitude so that the total mean square normalized density and vorticity perturbations, (ω_0, ρ_0) from **8** correspond to fluctuations of 10%. At $\mathcal{R}i = 5$, the basic mean flow from **4–6** has a period equal to 9 buoyancy times.

The evolution of representative density contours is depicted at times given by 1, 7, 8, and 9 periods, respectively, in Fig. 2. The slight density fluctuations in Fig. 2*A* have grown to substantial amplitude within the seven periods of motion depicted

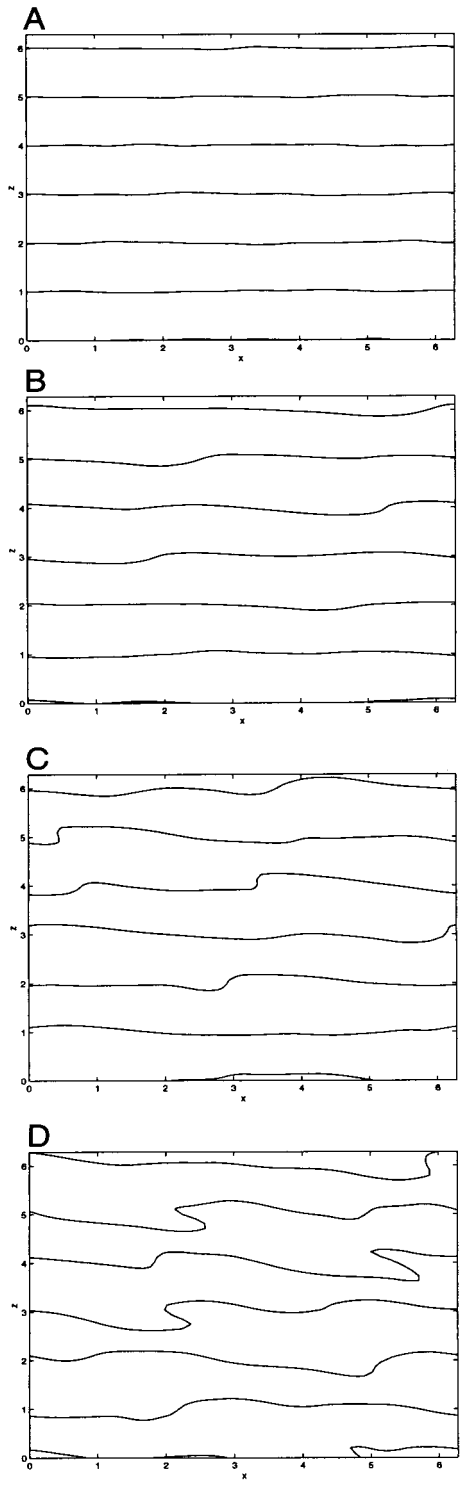

FIG. 2. Density contours at $t = 1, 7, 8, 9$ periods of mean flow, from top to bottom.

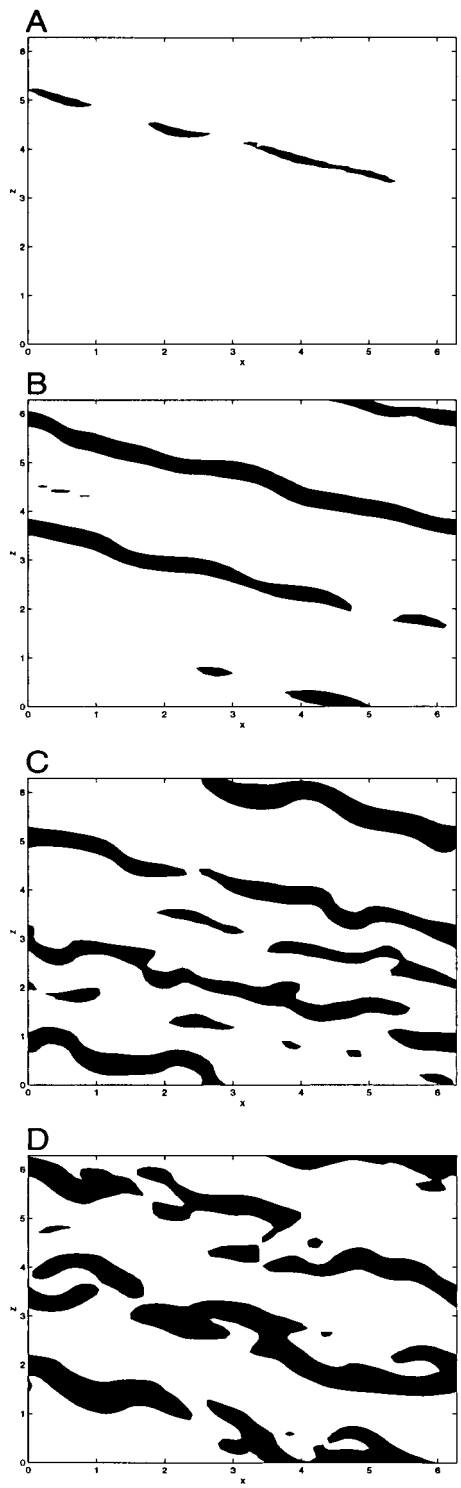

FIG. 3. Regions of overturning at $t = 8, 9, 11, 13$ periods of mean flow, from top to bottom.

in Fig. 2*B*; no density overturning occurs during this early stage. However, density overturning occurs between periods 7 and 8 of the mean motion with even more violent overturning evident by period 9 as depicted in Fig. 2*C* and *D*. To understand the nature of this overturning instability in a more quantitative fashion, we display the region of overturning at the period times, 8, 9, 11, and 13 in Fig. 3*A*, *B*, *C*, and *D*, respectively. The regions in black depict the locations with $\frac{d\bar{\rho}}{dz} > 0$, and there is local overturning. As is evident from Fig. 3*A* and *B*, the regions of overturning with this random initial data organize first into strips with a preferred angle of orientation and with strengthening velocity shear along these strips. The angle of orientation that emerges in Fig. 3*A* and *B* corresponds with high accuracy to the angle θ_0^* with strongest linearized instability depicted in Fig. 1*B* for $\mathcal{R}i = 5$. These regions of strong shear in a stratified flow are subject to Kelvin–

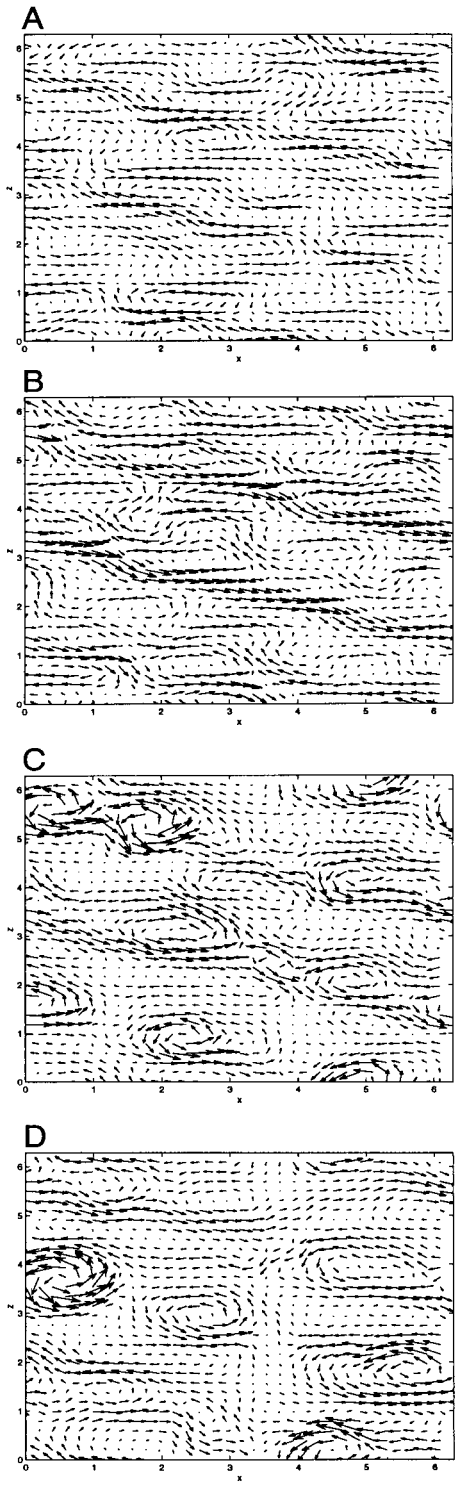

FIG. 4. Velocity field at $t = 8, 9, 11, 13$ periods of mean flow, from top to bottom.

Helmholtz instability (8) and this is exactly what can be inferred from Fig. 3*C* and *D* at the period times 11 and 13; this is especially evident for the center region of overturning in Fig. 3*D*. Plots of the velocity field, depicted in Fig. 4*A*, *B*, *C*, and *D* at the period times 8, 9, 11, and 13, show the formation of coherent like signed vortices consistent with such Kelvin–Helmholtz billows in these regions.

Discussion

In contrast to conventional expectations, we have developed a class of elementary time-periodic stratified flows and demonstrated their linearized instability at arbitrarily large Richardson numbers through unambiguous mathematical analysis. We have also presented numerical solutions for the nonlinear development of these instabilities with random initial data that confirm the predictions of linear theory and, significantly, indicate that their nonlinear instability leads to substantial density overturning and mixing. From the evidence presented here, we conjecture that such instabilities in these and related flow fields at large Richardson numbers may contribute significantly to the step-like microstructures often observed in buoyancy measurements in the ocean (9, 10). Furthermore, these mechanisms with spontaneous generation of instability are fundamentally different from the traditional ones involving larger amplitude gravity wave breaking (11).

To understand the robustness of the phenomena presented here and its potential physical significance, it is important to understand three-dimensional effects, the role of viscosity and heat conduction, and the occurrence of similar instabilities in a wider class of elementary stratified flow fields. A more complicated direct Eulerian linearized stability analysis that addresses all of these issues has been developed elsewhere by the authors (12). Clearly, more numerical simulations in both two and three space dimensions are needed to address the nonlinear effect of the instabilities developed here on both density overturning and mixing.

A.J.M. is partially supported by research grants NSF DMS-9625795, ONR N00014-96-0043, ARO DAAH04-95-1-0345. M.S. is supported as a post-doc by grants NSF DMS-9625795 and ONR N00014-96-0043.

1. Miles, J. W. (1961) *J. Fluid Mech.* **10,** 496–508.
2. Howard, L. N. (1961) *J. Fluid Mech.* **13,** 158–160.
3. Smagorinsky, J. (1963) *Mon. Weather Rev.* **91,** 99–164.
4. Lilly, D. K. (1967) *Proc. IBM Sci. Comput. Symp. Environ. Sci.*, 195–210.
5. Magnus, W. & Winkler, S. (1979) *Hill's Equation* (Dover, New York).
6. Hochstadt, H. (1975) *Differential Equations* (Dover, New York).
7. E, W. & Shu, C. (1994) *Phys. Fluids* **6,** 49–58.
8. Klassen, G. P. & Peltier, W. R. (1985) *J. Atmos. Sci.* **42,** 1321–1339.
9. Barenblatt, G. I. (1996) *Scaling, Self-Similarity and Intermediate Asymptotics* (Cambridge Univ. Press, Cambridge, U.K.).
10. Gregg, M. C. (1987) *J. Geophys. Res.* **92,** 5249–5286.
11. Lombard, P. N. & Riley, J. J. (1996) *Dyn. Atmos. Oceans* **23,** 345–355.
12. Majda, A. & Shefter, M. (1998) *J. Fluid Mech.*, in press.